Possible Al−F Bonding Environment in Fluorine-Bearing Sodium Aluminosilicate Glasses: From Calculation of ^{19}F NMR Shifts

Yun Liu* and John Tossell

Department of Chemistry and Biochemistry, University of Maryland, College Park, Maryland 20742

Received: April 17, 2003; In Final Form: July 14, 2003

A method that uses both Hartree−Fock and hybrid Hartree−Fock density functional methods at the 6-311+G-(2df,p) basis set level is used to calculate the ^{19}F NMR chemical shifts for possible Al−F species in sodium aluminosilicate glasses. The accuracy of this method has been carefully checked by calculating ^{19}F NMR shifts for several well-characterized crystalline materials. Almost all possible Al−F bonding environments in sodium aluminosilicate glasses, including terminal F atoms, corner-shared F species (i.e., both Al−F−Al or Al−F−Si), and edge-shared F species (i.e. Al−(FF)−Al), in 4-, 5-, and 6-coordinated Al species have been investigated. A clear trend is observed between the chemical composition of the environment and the F NMR shift. With more and more bridging O atoms in the vicinity, the F atom becomes less shielded, regardless of whether it is terminal or shared. Both Na^+-free and Na^+-bearing cluster models are used to investigate both this trend and the change in chemical-shift values upon Na^+ addition. Terminal F atoms are highly shielded, with chemical shifts from −172 ppm to −216 ppm. Corner-shared F atoms have a broad chemical-shift distribution, from −104 ppm to −197 ppm. Edge-shared F species have chemical shifts from −143 to −172 ppm. Many shared F environments could possibly contribute to the −147 ppm broad peak that is reported in the ^{19}F NMR spectra of fluorine-bearing aluminosilicate glasses.

1. Introduction

Because of strong electron correlation effects, the calculation of ^{19}F NMR shifts has been a difficult task for a long time. Both the Hartree−Fock (HF) method and the density functional theory (DFT) methods often give poor results for ^{19}F shifts.[1,2] The Moller−Plesset second order-perturbation theory (MP2) NMR method[3] gives somewhat more-accurate results; however, it is extremely time-consuming, and its results still do not accurately match the experimental results. Recently, an empirical scaling method that was suggested by Liu and Nekvasil, using results of both HF and B3LYP methods, successfully predicted the ^{19}F NMR chemical shifts in several gas-phase molecules and aluminosilicate systems.[4] This method is actually similar in approach to a method that was developed by Handy and coworkers;[5] their method combined HF and DFT methods. Here, the scaling method of Liu and Nekvasil is used to investigate possible species in fluorine-bearing aluminosilicate glasses.

Fluorine strongly affects the density and viscosity of silicate melts, fluid/melt partition coefficients of trace elements, mineral/melt equilibrium, and cation diffusion rates in melts.[6−12] These effects are very important to fields such as ceramic sciences and geosciences. Fluorine-bearing aluminosilicate glasses (oxyfluoride glasses) are promising materials for telecommunication applications, because of their optical transparency, low phonon energies, and rare-earth-ion solubilities.[13−15] Hence, the study of fluorine-bearing species in such systems may help us understand those significant properties.

For aluminosilicate glasses, it is well accepted that fluoride bonds preferentially with aluminum. Evidence for this comes from many areas, such as phase-diagram studies,[10,11] Raman spectroscopic studies,[12] and NMR studies.[13−18] Using ^{27}Al NMR, Kohn et al. concluded that the results of their ^{19}F to ^{27}Al cross-polarization MAS NMR experiments indicated the presence of 4-, 5-, and 6-coordinated fluorine-bearing Al species in sodium aluminosilicate glass.[16] Using ^{19}F NMR, Schaller et al. suggested that the major fluorine-bearing species in sodium aluminosilicate glass is the "cryolite-like" AlF_6^{3-} octahedron.[17] Many other researchers agreed that the major Al−F species are 6-coordinated, cryolite-like species that have isolated AlF_6^{3-} octahedra, probably surrounded by Na^+ cations.[16,18]

However, less of a consensus has been reached on the possible existence of small amounts of Si−F linkages. This controversy has primarily involved the potential assignments of the second large peak in the ^{19}F NMR spectra of some sodium aluminosilicate glasses that is centered at −147 ppm.[17,18] Although Schaller et al. found no indications in their ^{19}F to ^{29}Si CP/MAS results that suggested Si−F bonding, Zeng and Stebbins said that it was difficult to exclude Si−F bonding by such experiments if such bonding involves only a small number of Si sites in an amorphous system. Zeng and Stebbins further noted that the peak centered at −147 ppm was close to −152 ppm, which is the position of Si−F−Na(n) groups in crystalline Na_2SiF_6. In addition, given Duncan et al.'s assignment of the −139 ppm peak in fluorine-doped SiO_2 glass to [Si(O_3-)F] species,[19] Zeng and Stebbins suggested that the Na_2SiF_6-like species, as well as 4-coordinated Si species, could contribute to the peak at −147 ppm. Other data exist that are consistent with the formation of Si−F bonds. For example, the presence of Si−F bonding can better explain the decrease in viscosity that is observed when fluorine is added to aluminum-free systems.[7,20,21]

In previous work, Liu and Nekvasil agreed with the Si−F bonding assignment to the −147-ppm peak, on the basis of NMR calculations for some Si−F species.[4] They found that not only [Si(O_3-)F] and Na_2SiF_6-like species, but several other Si−F

* Author to whom correspondence should be addressed. E-mail: yunliu@glue.umd.edu.

10.1021/jp0350417 CCC: $25.00
Published on Web 09/19/2003

TABLE 1: Calculated and Experimental ^{19}F NMR Results for Crystalline Phases[a]

	^{19}F NMR Result (ppm)				
phase	HF	B3LYP	scaled	experimental (chemical shift)	reference
$Na_5Al_3F_{14}$[b] (chiolite,151.2°)	−141.6	−179.2	−160.4	−165	Du et al.[35]
Na_2SiF_6[b]	−129.6	−177.0	−153.3	−152	Du et al.[35]
K_2SiF_6	−117.6	−156.1	−136.9	−136	Kiczenski and Stebbins[36]
LiF	−178.0	−220.0	−199.0	−204	Miller[37]
NaF	−193.3	−250.9	−222.1	−225	Schaller et al.[17]
KF	−126.1	−142.8	−134.5	−132.4	Burum et al.[38]

[a] The clusters used to calculate these crystalline phases are shown in Figure 1. All the cluster structures are built using X-ray experimental coordinates. [b] Results have been taken directly from the work of Liu and Nekvasil.[4]

species (including 5-coordinated species, e.g., SiF_5^-), could easily produce the −147-ppm peak if they are present in the system. They also could exclude all the Al−F species they had tested as possible assignments for that peak. However, their calculations on the Al−F species were focused only on terminal F atoms and pure aluminum fluorides in various 4-, 5-, and 6-coordinated Al species. However, O and F mixed-coordinated Al complexes (oxyfluoride species) may be important, in regard to the glasses, and we need to check their F NMR shifts also. Hence, here, we present a further comprehensive study that is focused on those O and F mixed-coordinated Al species, especially those with bridging F atoms (Al−F−Al or Al−F−Si).

2. Calculation Methods

2.1. Geometry Optimization. All geometry calculations were performed using Gaussian 98.[22] Potential energy minima were located with the Berny algorithm, using redundant internal coordinates.[23] All geometry calculations used the B3LYP DFT method: Becke's three-parameter hybrid functional, using the LYP correlation functional method.[24] The chosen basis set was the standard polarized split-valence 6-31G* basis set, because the geometry results of the 6-31G* basis set often have an accuracy equivalent to that of much-larger basis sets.[25]

2.2. NMR Methods. NMR shielding tensor calculations were performed using the gauge-including atomic orbital (GIAO) method (the ab initio version that was first published by Ditchfield).[26] The GIAO method, which was used as the default NMR method in Gaussian 98, because of its faster convergence (Wolinski et al.),[27] computes chemical shieldings for nuclei on the basis of coupled perturbation theory that involves solving for the second derivative of the energy, with respect to the magnetic field and the magnetic moment of the nucleus (e.g., see the review by Tossell).[28]

Using the GIAO formalism, the isotropic shielding (σ_{iso}) is obtained by averaging the three principal tensor components σ_{11}, σ_{22}, and σ_{33}. Isotropic chemical shifts (δ_{iso}) were calculated using the relationship $\delta_{iso} = \sigma_{iso}^{ref} - \sigma_{iso}^{molecule}$, where σ_{iso}^{ref} is the chemical shielding value of a reference substance (chosen here to be $CFCl_3$ for ^{19}F), calculated at the same level. All the NMR calculations used the 6-311+G(2df,p) basis set. Although this is a rather large basis set, requiring long calculation times for some of the clusters, it is necessary to achieve the accuracy desired, as we will show using calculations on well-characterized crystalline solids.

2.3. Considerations for ^{19}F NMR Calculations. A F atom with three lone-pair electrons in its valence shell is expected to have strong electron correlation effects. That is the reason calculation of F NMR shifts is always difficult. As previously noted, HF- and DFT-level NMR calculations on the F atom can often show poor results. We found that the DFT methods seem to greatly overestimate electron correlation effects, yielding shielding values that are too small. In contrast, the HF methods have a tendency to yield shielding values that are too large. To explain this phenomenon, Tossell and Lazzeretti noted that the chemical shift is mainly determined by the paramagnetic contribution (Schreckenbach reached a similar conclusion later).[29−31] HF theory overestimates the highest occupied molecular orbital−lowest unoccupied molecular orbital (HOMO−LUMO) gap, because the LUMO energy corresponds to a system with $n + 1$ electrons. Pure DFT methods (such as LDA and GGAs), on the other hand, have been observed to underestimate the gap. Although a hybrid DFT method such as B3LYP has a "HF + pure DFT" combined exchange-correlation functional, it still has a smaller gap than the HF level. A smaller gap will induce less shielding, because stronger interaction between occupied and virtual orbitals will occur (because electrons can move more readily to unoccupied orbitals). Thus, it is likely that the "true" value of the energy difference lies somewhere between the values obtained by the DFT and HF methods. This situation opens the possibility of circumventing this problem by scaling the calculation results empirically. Certainly, it is possible that no linear relationship exists at all between the true value and the results of the HF and DFT methods (because each case has its unique electron correlation effects). Liu and Nekvasil suggested a linear scaling method that uses the average of the HF method and the hybrid B3LYP result.[4] Their results were compared with experimental data for many gas-phase fluorides and several crystalline materials. The method proved to be extremely accurate, which was definitely a big improvement, compared to HF or DFT method alone. Here, we further check this method by comparing calculated and experimental shifts for more crystalline fluorides that are related to the systems that we are studying (see Table 1 and Figure 1; the calculated F atoms are colored gray in all figures). Again, the calculated results using this scaling method are very good. There is a big improvement, in comparison to the results obtained using either the HF or B3LYP method alone (see Table 1). We think this scaling method is a rather reliable way to predict ^{19}F chemical shifts. Note that the method described in ref 5 is similar to that of Liu and Nekvasil. It is a method that is intermediate between the HF and B3LYP methods, although it is supported, to some extent, by theoretical rather than purely empirical arguments.

The accuracy of the method is shown by the results for crystalline compounds in Table 1. For the six compounds in the table, the root-mean-square error in the shift is only ∼3 ppm. The calculations reproduce even subtle effects, such as the difference between Na_2SiF_6 and K_2SiF_6 and the nonlinear trend in the series LiF, NaF, KF. The alkali fluorides have been previously treated in refs 32−34, using smaller clusters, less-robust basis sets, and either HF or DFT methods alone. Although

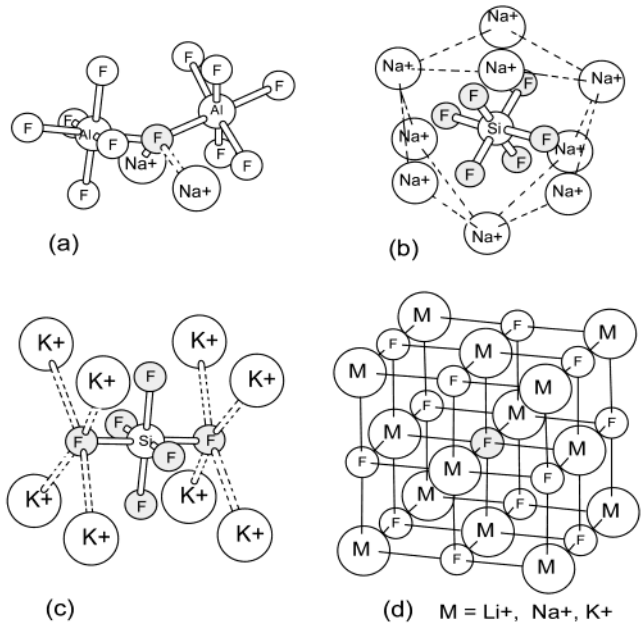

Figure 1. Cluster models used to calculate ^{19}F NMR for some crystalline materials from X-ray crystal data: (a) chiolite, (b) Na_2SiF_6, (c) K_2SiF_6, and (d) MF (where M = Li, Na, or K).

the results in refs 33 and 34 reproduce the nonlinear trend, they provide a much less accurate match to the experimental results. We have tested the importance of the basis set by repeating these calculations using the 6-311+G basis set, rather than the 6-311+G(2df,p) basis set. We have observed shifts of −220, −233, and −166 ppm for LiF, NaF, and KF, respectively, which gives the correct nonlinearity but much larger discrepancies, compared to experiment. Thus, larger clusters (larger than those used in refs 32−34), better basis sets, and the HF + B3LYP combination method are all important to getting accurate results.

2.4. Considerations for Cluster Models of Fluorine Glasses. Liu and Nekvasil gave detailed discussions on the effects of cluster size, Na^+ deshielding ability, and ∠T−O−T bond angles on F NMR shifts.[4] Here, we will present some of their conclusions: (i) the effective range for neighbor effects on the F NMR is, at most, 3.5 Å; and (ii) changing the ∠T−O−T bond angle near the F atom can only result in minor effects on the F NMR. In regard to the Na^+ deshielding ability, they found that the Na^+ cation showed only a very weak deshielding ability on Si−F species. However, the cases considered here are almost all Al−F species. The Na^+ deshielding ability in such species seems much stronger than that in Si−F species. For example, the SiF_6^{2-} cluster has a ^{19}F chemical shift of −154.3 ppm and the Na_2SiF_6 crystalline cluster model (see Figure 1b) has a shift of −153.3 ppm; the Na_2SiF_6 is only deshielded by 1 more ppm by the Na^+ cations that surround the SiF_6^{2-} cluster. However, the AlF_6^{3-} cluster has a ^{19}F chemical shift of −202 ppm, but if it is surrounded by four Na^+ cations and the geometry is optimized, the chemical shift of $(AlF_6-4Na)^+$ is deshielded by 8 ppm, to −194 ppm. This observation shows that the Na^+ ion has stronger deshielding ability on the F atom for the Al−F species. Hence, we need to investigate such deshielding effects if we want to know the exact chemical-shift values. Therefore, we must build our cluster models in two categories: (1) Na^+-free cluster models, which are used only for checking the pure chemical composition effects on F NMR shifts, to determine some trends; and (2) those with Na^+ clusters, which are used for accurate determination of the exact chemical shift for species, especially those which we think might give shifts close to the −147-ppm peak.

TABLE 2: Calculated Chemical Shifts for Terminal F Atoms in 4-, 5-, and 6-Coordinated Al Species

species	corresponding figure	^{19}F chemical shift (ppm)
AlF_4^-		−216
$AlF_3(OSiH_3)^-$		−211
$AlF_2(OSiH_3)_2^-$		−204, −207
$AlF(OSiH_3)_3^-$	2a	−201
AlF_5^{2-}		between −206 and −200
$AlF_4(OSiH_3)^{2-}$		between −204 and −198
$AlF_3(OSiH_3)_2^{2-}$	2c	−193, −150,[a] −150[a]
$AlF_2(OSiH_3)_3^{2-}$		−201, −180[a]
$AlF(OSiH_3)_4^{2-}$		−200
AlF_6^{3-}		−202
$AlF_5(OSiH_3)^{3-}$		unstable
$AlF_4(OSiH_3)_2^{3-}$		unstable
$AlF_3(OSiH_3)_3^{3-}$		unstable
$AlF_2(OSiH_3)_4^{3-}$		unstable
$AlF(OSiH_3)_5^{3-}$		unstable
$AlF_4^-\cdots Na^+$		−206
$AlF_4^-\cdots 2Na^+$		−204
$AlF_3(OSiH_3)^-\cdots Na^+$		between −207 and −203
$AlF_2(OSiH_3)_2^-\cdots Na^+$		−200
$AlF(OSiH_3)_{3-}\cdots Na^+$	2b	−195
$AlF(OSiH_3)_{3-}\cdots 2Na^+$		−193
$AlF_5^{2-}\cdots Na^+$		between −202 and −188
$AlF_5^{2-}\cdots 2Na^+$		between −198 and −189
$AlF_4(OSiH_3)^{2-}\cdots Na^+$		between −196 and −188
$AlF_3(OSiH_3)_2^{2-}\cdots Na^+$		between −188 and −181
$AlF_2(OSiH_3)_3^{2-}\cdots Na^+$	2d	−185, −172
$AlF(OSiH_3)_4^{2-}\cdots Na^+$		−177
$AlF_6^{3-}\cdots 4Na^+$		−194

[a] Because we use H atoms at the cut-off places as charge balancers, these values are obviously affected by F···H hydrogen bonding and should be ignored.

3. Results and Discussion

F atoms in aluminum compounds can be located at terminal positions, bonding to only one Al atom, or at shared positions, linking two Al atoms (or Al−F−Si). Before we begin to study the many possible bonding situations below, one more thing must be noted: although there is no hydrogen in the real glass systems that we are studying, our cluster models use "$OSiH_3$" ligands to represent some fragments of the glass network. That is because the distance between the F atom of interest and the $[SiO_4]$ tetrahedron usually is >3.5 Å, so that using a "$OSiH_3$" or $[SiO_4]$ to represent the real Si tetrahedron will not bring any noticeable difference for ^{19}F NMR. Hence, the "$OSiH_3$" in our cluster models actually represents a $[SiO_4]$ tetrahedron. We have tested this assumption for some cases; for example, we have calculated the ^{19}F shift for the $AlF[OSi(OH)_3]_3^-$ species for comparison with that for the $AlF(OSiH_3)_3^-$ species in Table 2, finding values of −196 ppm for the larger cluster with −OH termination and −201 ppm for the smaller cluster with −H termination (in our view, the smaller −H termination species are even better, because −OH terminated species often experience a greater deshielding effect by unreal F···H hydrogen bonding).

3.1. Terminal F Species. Terminal F atoms can be present in 4-, 5-, and 6-coordinated Al species. The experimental ^{27}Al NMR results did not show any other possible coordination situations.[16,39] Table 2 lists many of these terminal F-atom bonding situations and their ^{19}F NMR results with and without Na^+ cations. We always build the cluster models by following the Al avoidance rule, because even in glasses, there are almost no Al−O−Al linkages in such systems.[40] We use the following terminology. Here, $AlF(OSiH_3)_3^-$ represents a cluster in which one Al atom is coordinated by one terminal F atom and three

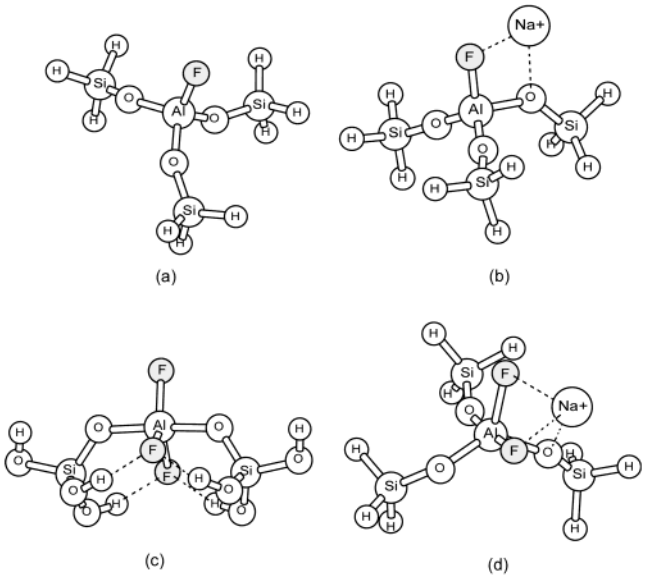

Figure 2. Cluster models used for the terminal F atom in 4-coordinated Al species.

bridging O (BO) atoms and each O atom is linked to another SiH_3 group tetrahedron (see Figure 2a). The expression "$AlF(OSiH_3)_3^-\cdots Na^+$" means that one Na^+ ion has been added to the previous species (see Figure 2b).

First, from the results for the sodium-free species (the top portion of data in Table 2), we see a very clear trend in the shielding, relative to composition. If a neighboring terminal F atom is substituted for a BO atom in the coordination shell of either a 4- or 5-coordinated Al−F species, the F atom will have a larger NMR shielding and, thus, a more negative shift. For instance, from $AlF(OSiH_3)_3^-$ to AlF_4^-, the chemical shift of the terminal F atom will change from −201 ppm to −216 ppm. Fluorine-bearing Al species that are 5-coordinated generally exhibit the same trend; one exception is $AlF_3(OSiH_3)_2^{2-}$ (see Figure 2c; some strong unreal hydrogen bonding occurs in that cluster). The terminal F atom in 5-coordinated Al−F cases can have different positions in the coordination shell (i.e., equatorial versus axial), giving slightly different chemical shifts. Because the substitution of a BO atom by a F atom also increases the shielding of the Al atom in both 4- and 5-coordinated clusters, there is a positive correlation between Al and F shielding.

Second, there is a spectrum in the distribution of ^{19}F NMR chemical shifts, and the 4-coordinated Al−F species occupy more-negative chemical-shift ranges, from −216 to −201 ppm. That observation means that 4-coordinated terminal Al−F species can be easily distinguished from the 5- and 6-coordinated

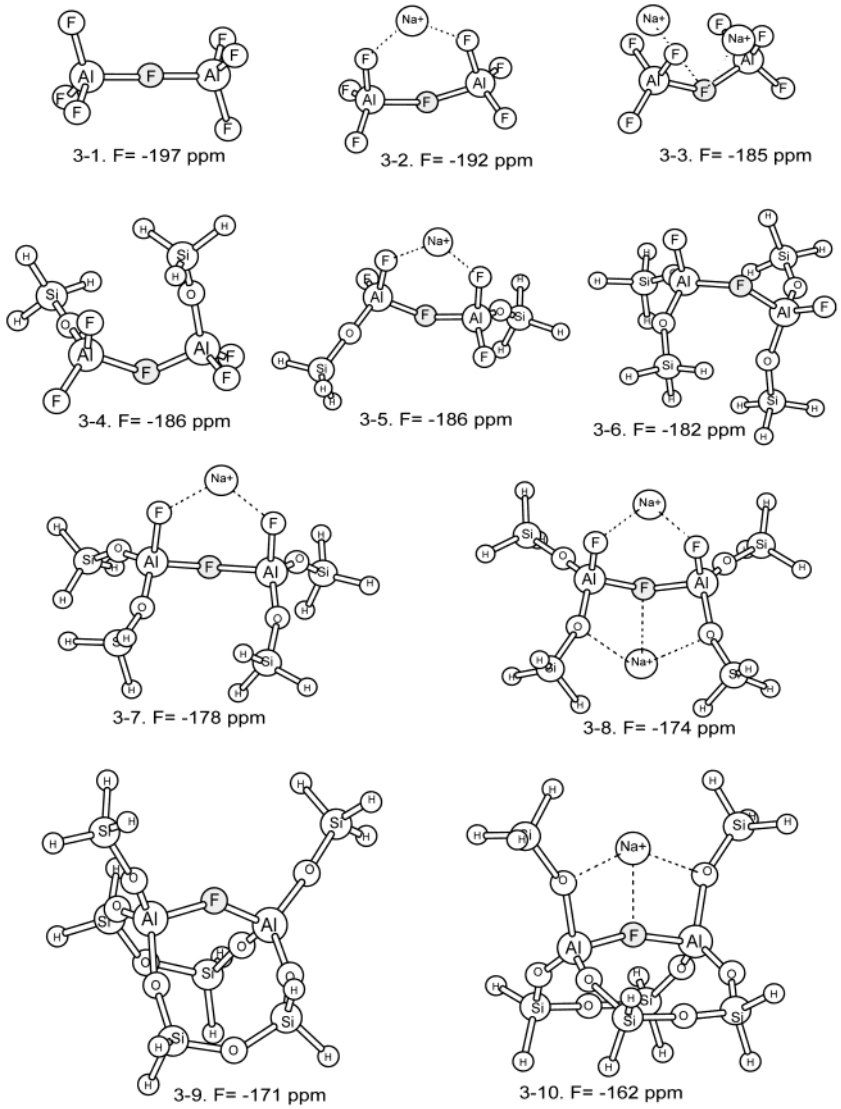

Figure 3. Cluster models used for corner-shared bridging F atoms in 4-coordinated Al species, and their chemical-shift values.

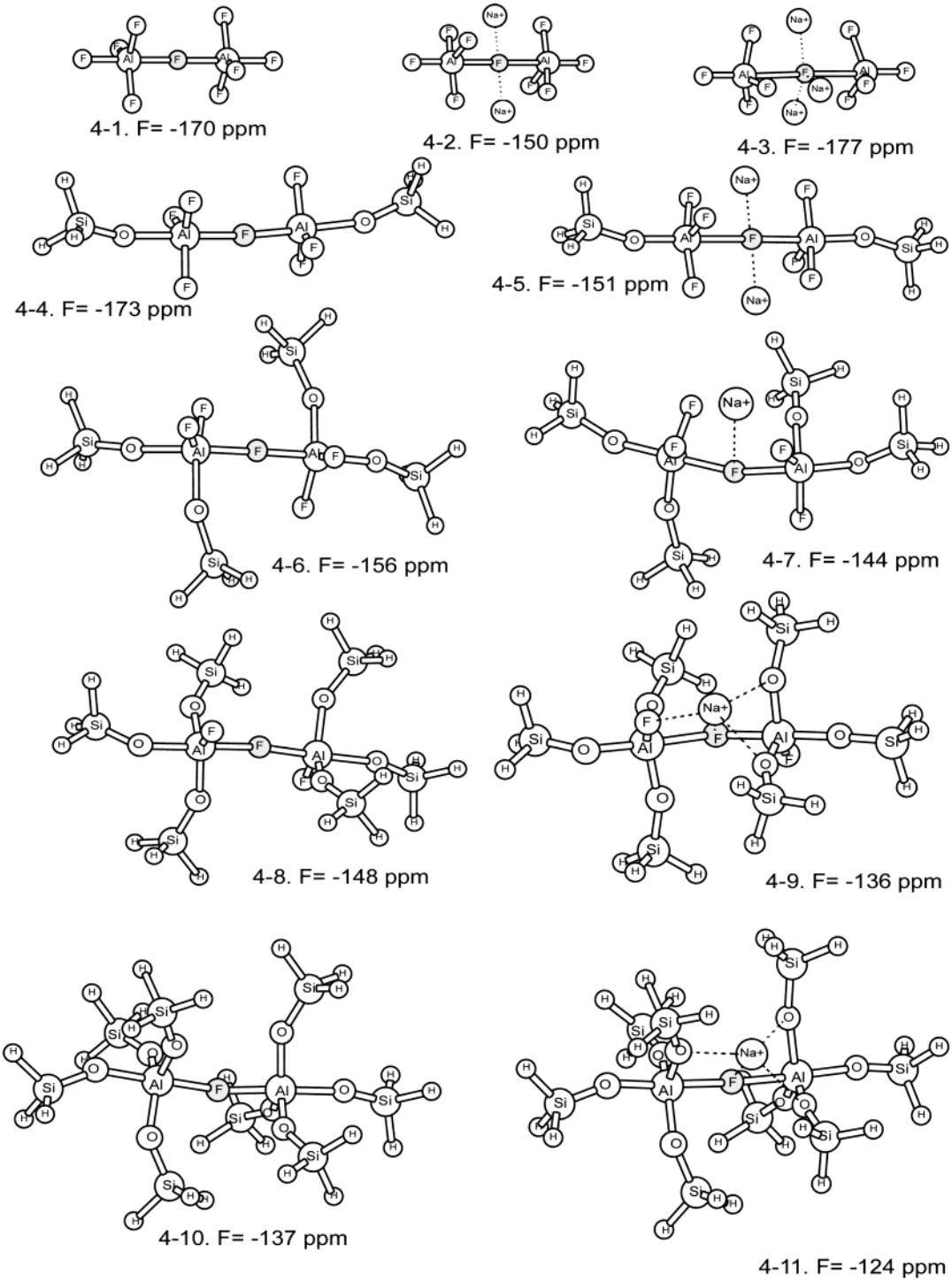

Figure 4. Cluster models used for corner-shared bridging F atoms in 5-coordinated Al species, and their chemical-shift values.

species. The 5- and 6-coordinated species have rather overlapping distributions of their F chemical shifts, from approximately −206 to −177 ppm. (This overlap is shown graphically in Figure 8 at the end of this paper.) Except for the pure fluoride AlF_6^{3-}, other terminal F atoms in 6-coordinated Al species (with some BO atoms) are all unstable during our geometry optimizations. They usually break up into 5-coordinated Al species or shared-F species.

All the sodium-free terminal F species produce a chemical shift at approximately −193 to −216 ppm. This is quite far from the −147-ppm F NMR peak region. Additional hydrogen bonding to those terminal F atoms can deshield them into the −147-ppm peak region if there are two strong hydrogen bonds (e.g., the $AlF_3(OSiH_3)_2^{2-}$ species; see Figure 2c). Except for the hydrogen bonding, as we have previously cited as a conclusion from Liu and Nekvasil,[4] other structural factors such as the Na^+ deshielding effect and the variation of the nearby ∠T−O−T bond angle simply cannot deshield the F atom that much (>40 ppm). Hence, we agree with what Liu and Nekvasil concluded: in *anhydrous* systems, all terminal F bonding environments in Al−F species cannot be assigned to the −147-ppm ^{19}F NMR peak.[4]

For accurate estimation of the Na^+ deshielding effects, we can also add one or more Na^+ cations surrounding the sodium-free species to see the actual effects. Table 2 lists several such results with the Na^+ cation. We see that, in most cases, the

cluster with added Na^+ cations can be deshielded by several parts per million; however, for some cases, deshielding values of even >20 ppm, compared to the Na^+-free cases (e.g., the $AlF(OSiH_3)_4^{2-}\cdots Na^+$ cluster versus the $AlF(OSiH_3)_4^{2-}$ cluster), are observed. In Table 2, the $AlF_6^{3-}\cdots 4Na^+$—a cluster that is similar to the cryolite—has a chemical shift at −194 ppm. The structure of cryolite is an isolated $[AlF_6^{3-}]$ octahedron surrounded by many Na^+ ions. Its experimental ^{19}F NMR chemical shift is −191 ppm.[17] Although our model does not correspond exactly to the cryolite situation, it is quite similar, and it shows that our prediction of deshielding is reasonable.

By adding Na^+ cations to all the terminal F species, the most-deshielded species we can obtain has a shift of approximately −172 ppm (see Figure 2d). Again, we do not believe any of these terminal F species can produce the −147-ppm peak.

3.2. Bridging F Species. There are two types of bridging F atoms. One is corner-shared (or single-shared), and the other is edge-shared (or double-shared).

3.2.1. Corner-Shared F Atoms in Al−F−Al Species. Figures 3, 4, and 5 respectively show all the cluster models for corner-shared 4-, 5-, and 6-coordinated species and their calculated ^{19}F NMR chemical-shift values. Because the ^{19}F NMR is not sensitive to the ∠T−O−T bond angle, we fix most of the ∠Al−O−Si bond angles to 150°, which is approximately the average ∠T−O−T bond angle in fluorine-bearing situations (with F atoms in the coordination shell, the ∠T−O−T bond angles have a tendency to be bigger than those fluorine-free aluminosilicate glass situations, which average ∼140°−144°).[39] Another reason to fix the bond angle is to avoid any unreal hydrogen bonding that may occur between the F atom and the charge-balancer H atom. As we previously mentioned, any bonding between the H atom and the F atom can cause significant deshielding effects.

From these results, we can see a clear trend in the ^{19}F NMR chemical-shift results versus the chemical composition. With more BO atoms in the vicinity, the corner-shared F atom (in gray color in all figures) will become less shielded, i.e., less-negative chemical shifts will be observed. For example, the ^{19}F NMR chemical shift of a corner-shared F atom in 4-coordinated Al−F species (see the Na^+-free species in Figure 3) will continuously change from −197 ppm, −186 ppm, and −182 ppm to −171 ppm with more and more BO atoms in the vicinity. The clusters with Na^+ cations just add additional deshielding effects to that trend. We also tested clusters with more than one Na^+ cation (i.e. see panels 3-3 and 3-8 in Figure 3), which bring deshielding effects to the corner-shared F atom that are several parts per million larger. The most deshielded situation for the corner-shared F atom in 4-coordinated Al species is that exhibited by panel 3-10 in Figure 3. Even here, the calculated chemical shift, at −162 ppm, is still not in the −147-ppm ^{19}F NMR peak region. Hence, we conclude that the −147-ppm peak in the ^{19}F NMR spectra is not caused by corner-shared F atoms in 4-coordinated Al species.

However, corner-shared F atoms in 5-coordinated Al species (see Figure 4) show the same trend of chemical shift, relative to composition. However, as more and more BO atoms are added, their shifts eventually reach the −147-ppm region. For determining the exact shielding values, it seems that putting one or two Na^+ cations around that F atom is sufficient. When we put 3 Na^+ cations around the F atom (i.e., panel 4-3 in Figure 4), the two Al atoms are pushed strongly away by the Na^+ cations and have a rather long Al−F−Al linkage, which might not be stable in real situations. Hence, the addition of one or two Na^+ cations to test the deshielding of that F atom is sufficient. From the shifts shown in Figure 4, we see that this type of corner-shared F atom in 5-coordinated Al−F species can have a chemical shift from approximately −170 ppm to −124 ppm in the real systems.

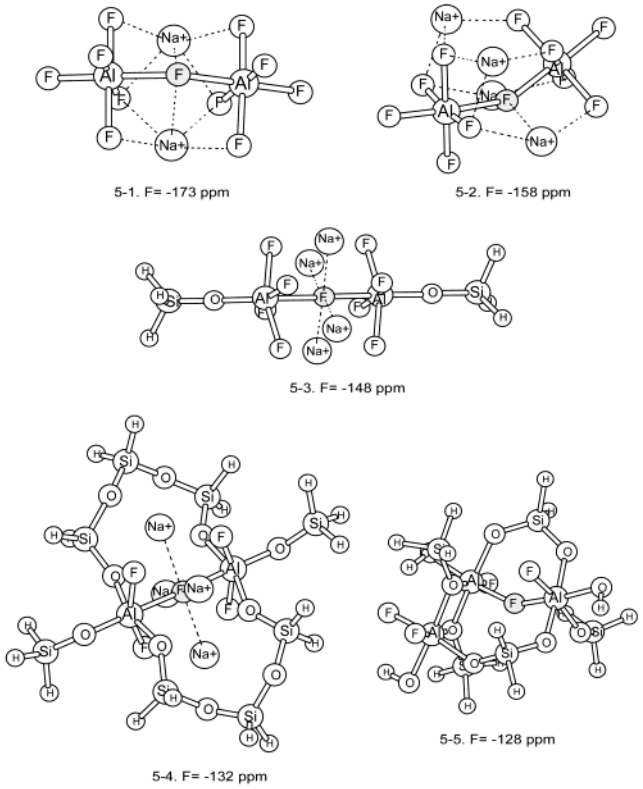

Figure 5. Cluster models used for corner-shared bridging F atoms in 6-coordinated Al species, and their chemical-shift values.

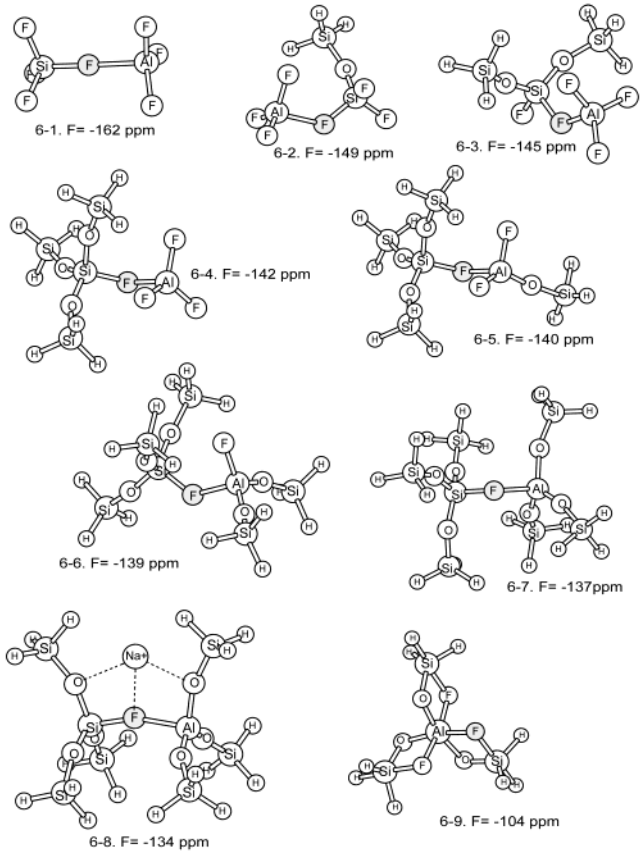

Figure 6. Cluster models used for corner-shared bridging F atoms in Al−F−Si species, and their chemical-shift values.

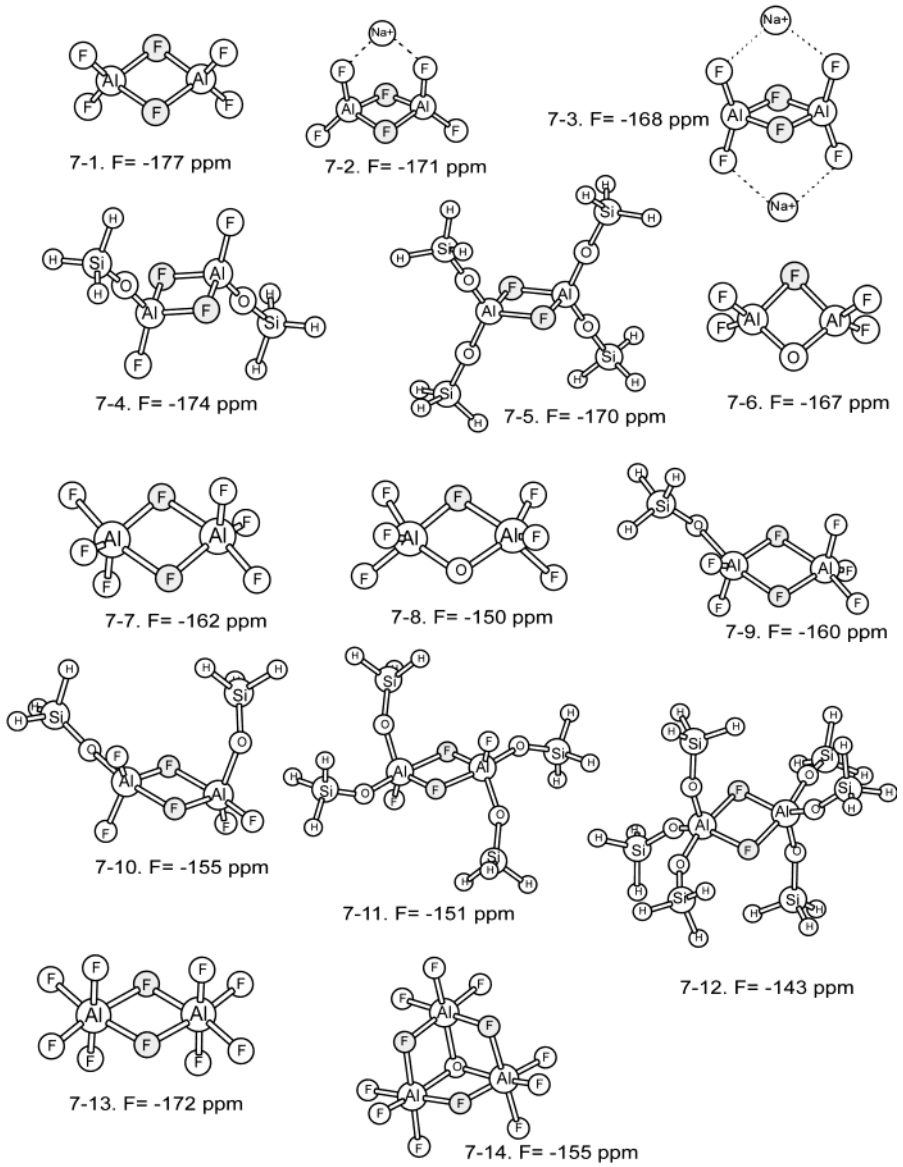

Figure 7. Cluster models used for edge-shared bridging F atoms in 4-, 5-, and 6-coordinated Al species, and their chemical-shift values.

Corner-shared F atoms in 6-coordinated Al cases are shown in Figure 5. Again, they show the same trend—the F atom gets less shielded as more BO atoms are present. We see that they also can easily have a chemical shift in the −147-ppm peak region. We think that such species can be present in the real systems in a significant amount. Some of them actually are fragments of well-known minerals; for example, panel 5-2 in Figure 5 is, indeed, a fragment of chiolite. With one more BO atom in each Al coordination shell (see panel 5-3 in Figure 5), the chemical shift of the F atom is almost −147 ppm. Panel 5-5 in Figure 5 is, in fact, a similar fragment of topaz but with two unshared F atoms. Topaz has a F-atom chemical shift value at approximately −142 ppm, and our cluster model gives a shift value of −128 ppm.

3.2.2. Corner-Shared F Atoms in Al−F−Si Species. Al−F−Si species may be present in the glasses. We have tested some such bonding situations, as shown in Figure 6. Most cases of 5- or 6-coordinated Al−F−Si corner sharing are unstable during the geometry optimization. Hence, we only have 4-coordinated results and one double-shared result (see panel 6-9 in Figure 6). We see that they follow the same trend that we found previously for composition versus shielding. The only difference is that additional Na^+ cations cannot deshield the F atom as much as in the Al−F−Al corner-sharing species. For example, the Na^+ cation can only deshield one species 3 ppm (see panels 6-7 and 6-8 in Figure 6).

We do not know whether this type of Al−F−Si linkage will be stable in the real systems. If they are, their ^{19}F NMR chemical shift will be in the range of −134 to −162 ppm. Also, the electric field gradients (EFGs) for aluminum in such Al−F−Si species are very large. This phenomenon causes the quadrupole coupling constants for aluminum to be large (∼27 MHz), which means that it is difficult to detect such species in ^{27}Al NMR spectra.

3.2.3. Edge-Shared F Atoms. Figure 7 shows the cluster models and their chemical-shift values for edge-shared F atoms in 4-, 5-, and 6-coordinated Al species. Again, they have the same trend as that previously observed. With more BO atoms, the F atom becomes less shielded and its chemical-shift values become less negative (e.g., from −177 ppm in panel 7-1 to −170 ppm in panel 7-5 of Figure 7). The Al−(FO)-Al bonding environments (e.g., panels 7-6, 7-8, and 7-14 of Figure 7) can dramatically deshield the F atom. Species with F atoms in such edge-sharing environments have recently been produced by F-atom substitution on the $GaAl_{12}$ polyoxocation species in solution.[41]

TABLE 3: Chemical-Shift Anisotropy of Terminal and Bridging F Atoms in Al−F Species[a]

species	corresponding figure	Chemical-Shift Anisotropy, CSA[a] (ppm) HF	B3LYP	average
$AlF(OSiH_3)_3^-$	2a	58.6	71.1	64.9
$AlF(OSiH_3)_3^-\cdots 2Na^+$		35.4	46.2	40.8
$AlF_2(OSiH_3)_2^-$		58.1, 62.2	69.7, 75.9	63.9, 69.1
$AlF_2(OSiH_3)_2^-\cdots Na^+$		41.3, 41.6	52.2, 52.4	46.8, 47.0
$AlF_3(OSiH_3)^-$		59.8	72.2	66
AlF_4^-		58.6	71.3	65.0
$F_3Al-F-AlF_3$	panel 3-1 in Figure 3			
terminal		64.4	78.1	71.3
bridging		72.1	89.9	81
$F_2OAl-F-AlOF_2$	panel 3-4 in Figure 3			
terminal		63	77	70
bridging		52.9	65.3	59.1
$F_2OAl-F-AlOF_2\cdots Na^+$	panel 3-5 in Figure 3			
terminal		52.3(×2)	61.7	57
terminal		68.6(×2)	83.5	76.1
bridging		67.8	82.9	75.4
$FO_2Al-F-AlO_2F$	panel 3-6 in Figure 3			
terminal		64.8	78.9	71.9
bridging		58.5	71.4	65.0
$FO_2Al-F-AlO_2F\cdots 2Na^+$	panel 3-8 in Figure 3			
terminal		56.8	66.3	64.1
bridging		58.3	71.4	64.9
$AlF_2O_3(SiH_3)_3^{2-}$		44.4, 50.3	55.9, 61.5	50.2, 55.9
$AlF_4OSiH_3^{2-}$		46.7(×3), 45.1	59.7(×3), 58.4	53.2(×3), 51.8
AlF_5^{2-}		46.3(×3), 45.7(×2)	60.5(×3), 64.0(×2)	53.4(×3), 54.9(×2)
$F_4Al-F-AlF_4$	panel 4-1 in Figure 4			
terminal		47	62	54.5
bridging		69.3	90.1	79.7
$F_4Al-F-AlF_4\cdots 3Na^+$	panel 4-3 in Figure 4			
terminal		43.2(×3)	51.8(×3)	47.5(×3)
terminal		63.9	77.4	70.7
bridging		19.0	38.3	28.7
$F_3OAl-F-AlOF_3\cdots 2Na^+$	panel 4-5 in Figure 4			
terminal		35.4−44.1	43.2−54.6	39.3−49.4
bridging		58.2	78.5	68.4
$F_2O_2Al-F-AlO_2F_2$	panel 4-6 in Figure 4			
terminal		49	60	54.5
bridging		60.5	76.3	68.4
$F_2O_2Al-F-AlO_2F_2\cdots Na^+$	panel 4-7 in Figure 4			
terminal		39.6−49.3	48.6−60.3	44.1−54.8
bridging		65.4	84.5	75.0
$FO_3Al-F-AlO_3F$	panel 4-8 in Figure 4			
terminal		50.3	61.1	55.7
bridging		69.2	83.8	76.5
$O_4Al-F-AlO_4$	panel 4-10 in Figure 4	65.6	78.5	72.1
$F_5Al-F-AlF_5\cdots 2Na^+$	panel 5-1 in Figure 5			
terminal		36.2−51.9	47.8−69.1	42−60.5
bridging		55.8	73.2	64.5
$F_4OAl-F-AlOF_4\cdots 4Na^+$	panel 5-3 in Figure 5			
terminal		36.7	44.1	40.4
bridging		46.6	53.6	50.1
$F_3Si-F-AlF_3$	panel 6-1 in Figure 6			
terminal		72(×3)	88.8(×3)	80.4(×3)
terminal		99.8(×3)	117.4(×3)	108.6(×3)
bridging		95.3	116.8	106.1
$O_3Si-F-AlF_3$	panel 6-4 in Figure 6			
terminal		58.0−72.2	70.1−89.3	64.1−80.8
bridging		71.9	85.8	78.9
$O_3Si-F-AlO_3$	panel 6-7 in Figure 6	83.4	99.4	91.4
$FO_2Al-FF-AlO_2F$	panel 7-11 in Figure 7			
terminal		54.0	66.1	60.1
bridging		46.8	57.4	52.1

[a] Abbreviations in table are as follows: (×2), two F atoms with the same value; and (×3) three F atoms with the same value.

In the absence of further Na^+ deshielding effects, the edge-shared bonding environments can have a chemical shift from −177 ppm to −143 ppm, which is similar to the −147-ppm peak that has been reported in the F NMR spectra for sodium aluminosilicate glasses.

From our aforementioned results, we see that many factors beyond the closest coordination shell of the F atom can significantly affect the ^{19}F NMR properties. Kiczenski and Stebbins suggested that the ^{19}F NMR data can be classified using the closest coordination shell of the F atom.[36] For example, Al−F−Na(3) means a local environment of the F atom that is linked to one Al atom and has three surrounding Na^+ ions. This environment can be easily distinguished from other environments, such as Al−F−Na(4) or Si−F−Na(2). However, our

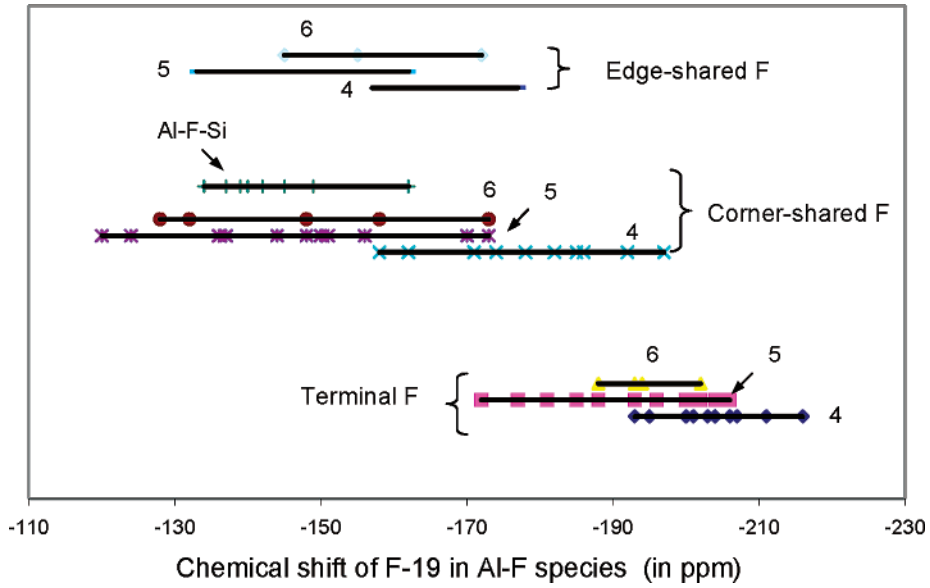

Figure 8. Diagram of the distribution of calculated ^{19}F chemical shifts for terminal, corner-shared, and edge-shared F atoms in various aluminum-containing species. Numbers in the figure specify 4-, 5-, or 6-coordinated Al species.

study shows that different Al coordination (e.g. 4- or 6-coordinated) in the Al−F−Na(3) situation will give a very different ^{19}F NMR. Even with the same coordination number for the Al atom, different chemical compositions in the Al coordination shell (e.g., the number of BO atoms) will cause a difference in the ^{19}F NMR properties. Hence, the composition of the environment farther away from the F atom must also be considered.

3.3. Chemical-Shift Anisotropy (CSA) Values. The chemical-shift anisotropy (CSA) is defined as

$$\Delta\sigma = \sigma_{33} - \frac{\sigma_{11} + \sigma_{22}}{2}$$

Here, σ_{11}, σ_{22}, and σ_{33} are the principal components of the nuclear shielding tensor. Although, in our glass systems, the F sites will be numerous, the CSA values may still be useful for some researchers. We list some calculated CSA values in Table 3. In the same way that we treat the chemical shift of fluorine, we use the average of the HF and B3LYP results for CSA. The data in Table 3 present some interesting points:

(1) The CSA for terminal or bridging F atoms can be easily decreased if cations (i.e., Na^+) are close to the F atom. For example, the CSA for the Na^+-free species $AlF(OSiH_3)_3^-$ is 64.9 ppm, whereas that for $AlF(OSiH_3)_3^-\cdots 2Na^+$ is 40.8 ppm. The closer the Na^+ cation is located to the F atom, the smaller the CSA of the F atom will be. We also find that hydrogen bonding on the F atom also has similar effects. This fact can be used to distinguish those similar F sites with or without nearby cations.

(2) Without Na^+ cations, in 5-coordinated Al−F species, the bridging F atom has a larger CSA than the terminal F atom. For example, the species in panel 4-1 of Figure 4 has a CSA of 79.7 ppm for the bridging F atom and 54.5 ppm for the terminal F atom. However, the appearance of Na^+ cations can change this point. For some extreme cases, such as the species in panel 4-3 of Figure 4, the bridging F atom will even have a smaller CSA.

(3) The CSA will be much greater in Si−F bonding situations than in pure Al−F situations. The species in panels 6-1, 6-4, and 6-7 of Figure 6 display this point very well. The terminal F bonding to the Si atom in panel 6-1 of Figure 6 has a largest CSA value, 108.6 ppm. This is a good way to distinguish the F−Al or F−Si bondings.

4. Summary

Except for terminal F species and the corner-shared F atom in 4-coordinated Al−F species, all other bridging F species can have a resonance in the region of the −147-ppm peak that has been reported in ^{19}F NMR spectra for sodium aluminosilicate glasses. This finding means that the previous assignment of Si−F bonding environments to the −147-ppm peak may not be correct. At a minimum, Si−F bonding environments are not the only environments that could contribute to that peak.

We also found a clear trend in the chemical composition, relative to the F-atom shielding. With more and more bridging O atoms, the F atom in the vicinity will become less and less shielded. The specific chemical shift and chemical-shift anisotropy values that we have calculated for the complete series of possible Al−F species will undoubtedly benefit those studying speciation in related glasses or minerals. The calculated ranges of ^{19}F NMR shifts are summarized in Figure 8.

Acknowledgment. This work was supported by the National Science Foundation (NSF Grant No. EAR-0001031) and the U.S. Department of Energy (DOE Grant No. DE-FG02-94ER14467). Some of the calculations were performed using Gaussian 98 on the Carnegie Alpha Cluster, which is supported, in part, by NSF MRI Grant No. AST-9976645. We also want to thank Dr. Bjorn O. Mysen and Dr. George D. Cody for helpful discussions on the issue of the ^{19}F NMR of aluminosilicate glasses.

References and Notes

(1) Cheeseman, J. R.; Trucks, G. W.; Keith, T. A.; Frisch, M. J. *J. Chem. Phys.* **1996**, *104*, 5497−5509.

(2) Wilson, P. J.; Amos, R. D.; Handy, N. C. *Mol. Phys.* **1999**, *97*, 757−768.

(3) Gauss, J. *J. Chem. Phys.* **1993**, *99*, 3629−3643.

(4) Liu, Y.; Nekvasil, H. *Am. Mineral.* **2002**, *87*, 339−346.

(5) Wilson, P. J.; Amos, R. D.; Handy, N. C. *Chem. Phys. Lett.* **1999**, *312*, 475−484.

(6) Dingwell, D. B.; Scarfe, C. M.; Cronin, D. J. *Am. Mineral.* **1985**, *70*, 80−87.
(7) Dingwell, D. B. *Am. Mineral*. **1989**, *74*, 333−338.
(8) Dingwell, D. B.; Knoche, R.; Webb, S. L. *Am. Mineral.* **1993**, *78*, 325−330.
(9) Snow, E.; Kidman, S. *Nature* **1991**, *349*, 231−233.
(10) Manning, D. A. C.; Hamilton, D. L.; Henderson, C. M. B.; Dempsey, M. J. *Contrib. Mineral. Petrol.* **1980**, *75*, 257−252.
(11) Manning, D. A. C. *Contrib. Mineral. Petrol.* **1981**, *76*, 206−215.
(12) Mysen, B. O.; Virgo, D. *Contrib. Mineral. Petrol*. **1985**, *91*, 205−220.
(13) Tran, D. C.; Sigel, G. H.; Bendow, B. *J. Lightwave Technol.* **1984**, *2*, 566−586.
(14) Ainslie, B. J.; Davey, S. T.; Szebesta, D.; Williams, J. R.; Moore, M. W.; Whitley, T.; Wyatt, R. *J. Non-Cryst. Solids* **1995**, *184*, 225−228.
(15) Youngman, R. E.; Dejneka, M. J. *J. Am. Ceram. Soc.* **2002**, *85*, 1077−1082.
(16) Kohn, S. C.; Dupree, R.; Mortuza, M. G.; Henderson, C. M. B. *Am. Mineral*. **1991**, *76*, 309−312.
(17) Schaller, T.; Dingwell, D. B.; Keppler, H.; Knoller, W.; Merwin, L.; Sebald, A. *Geochim. Cosmochim. Acta* **1992**, *56*, 701−707.
(18) Zeng, Q.; Stebbins, J. F. *Am. Mineral.* **2000**, *85*, 863−867.
(19) Duncan, T. M.; Douglass, D. C.; Csencsits, R.; Walker, K. L. *J. Appl. Phys.* **1986**, *60*, 130−136.
(20) Luth, R. W. *Am. Mineral.* **1988**, *73*, 306−312.
(21) Luth, R. W. *Am. Mineral.* **1988**, *73*, 297−305.
(22) Frisch, M. J.; Trucks, G. W.; Schlegel, H. B.; Scuseria, G. E.; Robb, M. A.; Cheeseman, J. R.; Zakrzewski, V. G.; Montgomery, J. A., Jr.; Stratmann, R. E.; Burant, J. C.; Dapprich, S.; Millam, J. M.; Daniels, A. D.; Kudin, K. N.; Strain, M. C.; Farkas, O.; Tomasi, J.; Barone, V.; Cossi, M.; Cammi, R.; Mennucci, B.; Pomelli, C.; Adamo, C.; Clifford, S.; Ochterski, J.; Petersson, G. A.; Ayala, P. Y.; Cui, Q.; Morokuma, K.; Malick, D. K.; Rabuck, A. D.; Raghavachari, K.; Foresman, J. B.; Cioslowski, J.; Ortiz, J. V.; Stefanov, B. B.; Liu, G.; Liashenko, A.; Piskorz, P.; Komaromi, I.; Gomperts, R.; Martin, R. L.; Fox, D. J.; Keith, T.; Al-Laham, M. A.; Peng, C. Y.; Nanayakkara, A.; Gonzalez, C.; Challacombe, M.; Gill, P. M. W.; Johnson, B. G.; Chen, W.; Wong, M. W.; Andres, J. L.; Head-Gordon, M.; Replogle, E. S.; Pople, J. A. *Gaussian 98*, revision A.9; Gaussian, Inc.: Pittsburgh, PA, 1998.
(23) Peng, C.; Ayala, P. Y.; Schlegel, H. B.; Frisch, M. J. *J. Comput. Chem.* **1996**, *17*, 49−56.
(24) Becke, A. D. *J. Chem. Phys.* **1993**, *98*, 5648−5652.
(25) Foresman, J. B.; Frisch, A. E. *Exploring Chemistry with Electronic Structure Methods*, 2nd ed.; Gaussian, Inc.: Pittsburgh, PA, 1996.
(26) Ditchfield, R. *Mol. Phys.* **1974**, *27*, (4), 789−807.
(27) Wolinski, K.; Hinton, J. F.; Pulay, P. *J. Am. Chem. Soc.* **1990**, *112*, 8251−8260.
(28) Tossell, J. A. In *Reviews in Mineralogy and Geochemistry*. Cygan, R. T., Kubicki, J. D., Eds.; The Mineralogical Society of America: Washington, DC, 2001; Vol. 42, pp 437−458.
(29) Lazzeretti, P.; Tossell, J. A. *J. Magn. Reson.* **1986**, *70*, 461−464.
(30) Tossell, J. A. *Chem. Phys. Lett.* **1986**, *132*, 464−466.
(31) Schreckenbach, G. *J. Chem. Phys.* **1999**, *110*, 11936−11949.
(32) Mortimer, M.; Moore, E. A.; Peirson, N. F. *J. Chem. Soc., Faraday Trans.* **1996**, *92*, 1117−1120.
(33) Cai, S.-H.; Chen, Z.; Xu, X.; Wan, H.-L. *Chem. Phys. Lett.* **1999**, *302*, 73−76.
(34) Cai, S. H.; Chen, Z.; Wan, H.-L. *J. Phys. Chem. A* **2002**, *106*, 1060−1066.
(35) Du, L. S.; Samoson, A.; Tuherm, T.; Grey, C. P. *Chem. Mater*. **2000**, *12*, 3611−3616.
(36) Kiczenski, T. J.; Stebbins, J. F. *J. Non-Cryst. Solids* **2002**, *306*, 160−168.
(37) Miller, J. M. *Prog. Nucl. Magn. Reson. Spectrosc.* **1996**, *28*, 255−281.
(38) Burum, D. P.; Elleman, D. D.; Rhim, W. K. *J. Chem. Phys.* **1978**, *68*, 1164−1169.
(39) Liu, Y.; Nekvasil, H. *Am. Mineral.* **2001**, *86*, 491−497.
(40) Dirken, P. J.; Kohn, S. C.; Smith, M. E.; van Eck, E. R. H. *Chem. Phys. Lett*. **1997**, *266*, 568−574.
(41) Yu, P.; Lee, A. P.; Phillips, B. L.; Casey, W. H. *Geochim. Cosmochim. Acta* **2003**, *67*, 1065−1080.